JOURNAL OF COMPUTATIONAL PHYSICS 101, 265–275 (1992)

A Fully Nonlinear, Mixed Spectral and Finite Difference Model for Thermally Driven, Rotating Flows

TIMOTHY L. MILLER

Earth Science and Applications Division, NASA/Marshall Space Flight Center, Hunstville, Alabama 35812

HUEI-IIN LU

Universities Space Research Association, NASA/Marshall Space Flight Center, Huntsville, Alabama 35812

AND

KAREN A. BUTLER

New Technology, Inc., NASA/Marshall Space Flight Center, Huntsville, Alabama 35812

Received April 3, 1991

A model which can simulate a variety of thermally driven, rotating flows in cylindrical and spherical geometries is described. The technique used to approximate the Navier–Stokes equations is finite difference in time and in the meridional plane, and spectral in the azimuthal direction. The model can calculate axisymmetric flow, linearized waves with respect to a fixed or a changing axisymmetric flow, nonlinear waves without wave–wave interaction, and fully nonlinear three-dimensional flow. Detailed numerical studies are made to reexamine the steady baroclinic wave case previously investigated by Williams [*J. Fluid Mech.* **49**, 417 (1971)] and by Quon [*J. Comp. Phys.* **20**, 442 (1976)]. With one or more harmonic waves added to the fundamental wave 5, the present model in fully nonlinear mode agrees very well with Williams. With only a single wave, disagreement exists between the present model and that of Quon on the amplitude of the wave and its effects on the azimuthal mean circulation. New studies on wavenumber selection using the present model indicate that the results for this case depend on the initial conditions.

1. INTRODUCTION

The study of nonlinear development of large-scale baroclinic instabilities is fundamental to atmospheric dynamics. According to the linear theory of Charney [1] and Eady [2], an equilibrium basic state consisting of a vertical shear of horizontal wind and a stable vertical stratification is unstable to perturbations of an appropriate wavelength range. As perturbations continue to grow, the eddy processes redistribute heat and momentum, thereby altering the instability (potential energy) of the existing basic state. Some of the nonlinear effects of baroclinic eddies upon the azimuthal mean flow has been known for some time in the theory of atmospheric general circulation (Lorenz [3]). Among these important effects are: (1) reducing the horizontal temperature gradient and hence reducing the vertical wind shear, (2) creating a thermally indirect mean meridional circulation (or Ferrell cell), and (3) increasing the downward extent of the westerly flow. Nonlinear development of baroclinic instability has been studied in various investigations, including numerical studies of the primitive equations on the sphere (e.g., Gall [4]).

Baroclinic instability can also be studied in a relatively pure form in laboratory experiments (e.g., Fowlis and Hide [5]). The most common configuration is a cylindrical annulus that contains a working fluid rotated about the axis of symmetry, which is vertical. Fluid flow is thermally driven by maintaining the temperatures of outer and inner sidewalls at constants T_o and T_i, respectively. Baroclinic instability ensues if the rotation rate (Ω) is large enough and if the temperature difference falls within a certain range (which is a function of Ω).

A case of steady-amplitude baroclinic wave flow (hereafter called a "steady wave") in the rotating annulus experiment was first studied numerically by Williams [6–8] using a three-dimensional finite difference model. His numerical results demonstrated strong nonlinear effects of baroclinic waves on the axisymmetric flow, including a reduction of the zonal jet by about 40% from the axisymmetric solution, a well organized formation of the Ferrell cell, and a prevailing westerly surface flow in the middle of the annulus. The meridional cross sections of flow fields from a two-dimensional (axisymmetric) model integration and those of

0021-9991/92 $5.00

azimuthal means from the three-dimensional integration are shown in Figs. 1 and 2. These were recalculated with the model described in this paper. The results shown are nearly identical with those of Williams. This steady-wave case is important because it is so well documented that it has been regarded as an important benchmark case for new models.

Quon [9] described a model which used finite differences in the meridional plane and a single Fourier mode in the azimuthal direction, and with which the Williams steady wave case was simulated. Quon presented results which agreed with those of Williams, and concluded that an accurate modeling of the steady-wave case of Williams can be achieved by considering only a single-wave feedback mechanism upon the azimuthal mean state. One can conclude from Quon's results that wave–wave interactions are not important for this particular case.

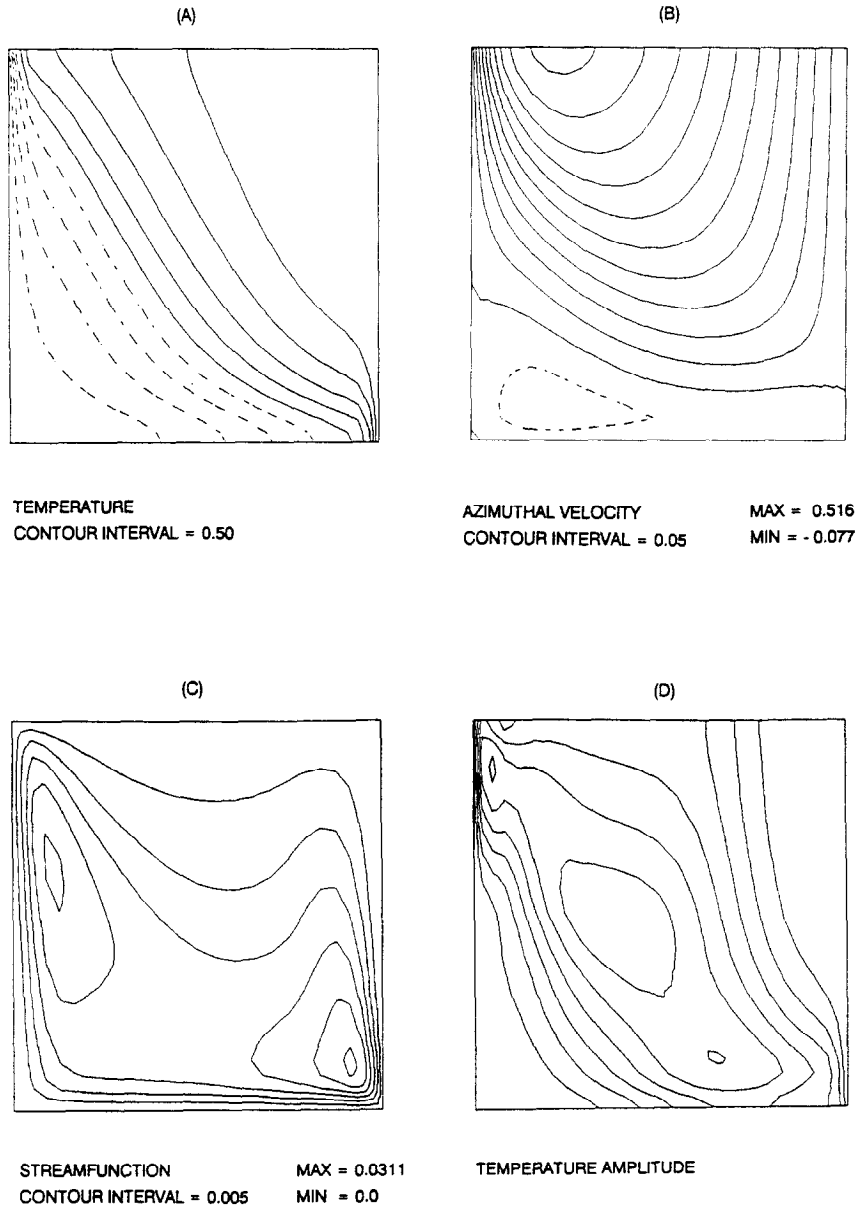

FIG. 1. Calculated steady axisymmetric solution (A)–(C) and linear eigenmode temperature amplitude structure (D): (A) Temperature deviation (°C); (B) azimuthal velocity (cm s^{-1}); (C) meridional streamfunction (cm^3 s^{-1}); (D) linear eigenmode temperature amplitude for wavenumber 5 (arbitrary units). Dashed contours are negative and the first solid contour is zero.

In the course of developing the present model which is capable of including multiple waves, the authors found a significant disagreement with the results of Quon [9]. While the simulation which include wave–wave interactions between waves 5 and 10 agrees with those of Williams, the simulation which includes only wave-mean flow interaction with a single wave 5 significantly underpredicts the amplitude of the wave and its effects upon the axisymmetric state. For example, only a 10% reduction in the zonal jet is obtained. It is the purpose of this paper to (1) describe the new numerical model, (2) document our disagreement with the results of Quon [9] and our agreement with those of Williams [6–8], and (3) report new results on the wavenumber selection as a function of initial conditions for the Williams case.

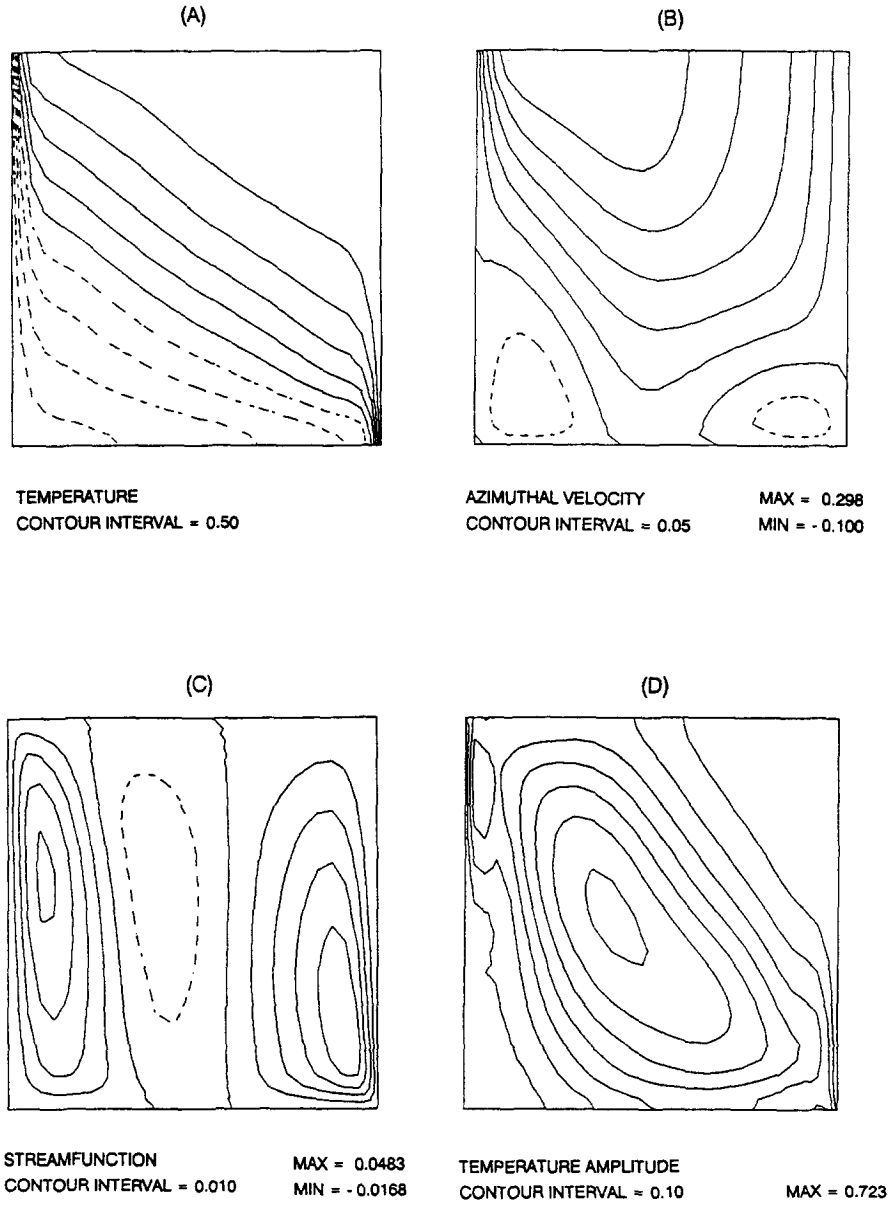

FIG. 2. Calculated azimuthal mean fields from the calculation which included waves 5, 10, and 15, and the temperature amplitude for wavenumber 5. Panels (A) through (C) are as in Fig. 1, panel (D) is in °C.

2. THE MODEL

2.1. *Equations and Boundary Conditions*

The present model is based upon the Boussinesq Navier–Stokes in rotating spherical coordinates. The symbols are listed in Table I.

$$\frac{\partial u}{\partial t} = -\left(\frac{1}{r\cos\phi}\frac{\partial}{\partial\phi}(uv\cos\phi) + \frac{1}{r^2}\frac{\partial}{\partial r}(wur^2) + \frac{1}{r\cos\phi}\frac{\partial u^2}{\partial\lambda}\right) + \frac{uv\tan\phi}{r} - \frac{uw}{r} + 2\Omega\sin\phi - 2\Omega w\cos\phi + \nu\left(\nabla^2 u - \frac{1}{r^2\cos^2\phi}\times\left[u + 2\frac{\partial}{\partial\lambda}(v\sin\phi - w\cos\phi)\right]\right) - \frac{1}{r\cos\phi}\frac{\partial\Pi}{\partial\lambda} \tag{2.1}$$

$$\frac{\partial v}{\partial t} = -\left(\frac{1}{r\cos\phi}\frac{\partial}{\partial\phi}(v^2\cos\phi) + \frac{1}{r^2}\frac{\partial}{\partial r}(wvr^2) + \frac{1}{r\cos\phi}\frac{\partial uv}{\partial\lambda}\right) - \frac{u\tan\phi}{r} - \frac{vw}{r} - 2\Omega u\sin\phi + \nu\left(\nabla^2 v - \frac{v}{r^2\cos^2\phi} + \frac{2\sin\phi}{r^2\cos^2\phi}\frac{\partial u}{\partial\lambda} + \frac{2}{r^2}\frac{\partial w}{\partial\phi}\right) - \frac{1}{r}\frac{\partial\Pi}{\partial\phi} \tag{2.2}$$

$$\frac{\partial w}{\partial t} = -\left(\frac{1}{r\cos\phi}\frac{\partial}{\partial\phi}(vw\cos\phi) + \frac{1}{r^2}\frac{\partial}{\partial r}(w^2r^2) + \frac{1}{r\cos\phi}\frac{\partial uw}{\partial\lambda}\right) + \frac{(u^2+v^2)}{r} + 2\Omega u\cos\phi + \nu\left(\nabla^2 w - \frac{2}{r^2\cos\phi}\frac{\partial}{\partial\phi}(v\cos\phi) - \frac{2}{r^2\cos\phi}\frac{\partial u}{\partial\lambda} - \frac{2w}{r^2}\right) + \beta gT - \frac{\partial\Pi}{\partial r} \tag{2.3}$$

$$\frac{\partial T}{\partial t} = -\left(\frac{1}{r\cos\phi}\frac{\partial}{\partial\phi}(vT\cos\phi) + \frac{1}{r^2}\frac{\partial}{\partial r}(wTr^2) + \frac{1}{r\cos\phi}\frac{\partial uT}{\partial\lambda}\right) + \kappa(\nabla^2 T). \tag{2.4}$$

TABLE I

List of Symbols

g	Body force ("gravity")
k	Longitudinal wavenumber
P	Pressure
r	Radial coordinate; distance from center of sphere
t	Time
T	Temperature
u	Azimuthal velocity (positive for westerly flow)
v	Meridional velocity (positive for southerly flow)
w	Radial velocity
β	Thermal expansivity
ϕ	Latitudinal coordinate
κ	Thermal diffusivity
λ	Longitudinal coordinate
Π	P/ρ_0
ρ_0	Reference density
ν	Kinematic viscosity
Ω	Rotation rate
ψ	Meridional streamfunction

The continuity equation is as follows:

$$\frac{1}{r\cos\phi}\frac{\partial}{\partial\phi}(v\cos\phi) + \frac{1}{r^2}\frac{\partial}{\partial r}(wr^2) + \frac{1}{r\cos\phi}\frac{\partial u}{\partial\lambda} = 0. \tag{2.5}$$

The cylindrical annulus is modeled in the spherical framework by using a very large spherical radius and considering the domain consisting of an annulus around the pole (Miller and Gall [10]). For the present case, we use the same boundary conditions as Williams [6–8] and Quon [9], namely, no-slip on the lower and side boundaries and free-slip on the upper surface. The temperatures on the inner and outer sidewalls are held constant, and the no heat flux condition is imposed on the top and bottom. As in the works of Williams and Quon, we assume that the upper free surface remains horizontal, ignoring the presence of centrifugal effects.

2.2. *Numerical Technique*

The model uses a mixed spectral and finite difference technique, similar to that used by Quon [9] for a cylindrical model. In the azimuthal direction, each field is decomposed into Fourier components of the form $A_k \exp(ik\lambda)$, where λ is longitude, k is wavenumber (0 for axisymmetric), and A_k is the complex amplitude of one of the dependent variables. By substituting the Fourier series for each variable into the governing equations (2.1)–(2.4) and operating on both sides by the orthogonalization procedure, one obtains a set of equations for each Fourier mode (Quon [9]). These equations can be systematically simplified to represent mathematical systems of different degrees of complexity. The present model is able to solve five classes of problems,

which are handled consistently with the same numerical algorithms:

(1) axisymmetric flow;

(2) linear instability problem with respect to a previously computed, fixed axisymmetric state;

(3) linear instability problem with respect to an evolving axisymmetric state as in (1);

(4) nonlinear problem for single and multiple waves, in which the only quadratic terms retained are those due to the interaction between the wave and axisymmetric parts of the flow (hereafter called wave-mean flow interaction); and

(5) fully nonlinear problem for multiple waves with complete wave-mean and wave-wave interactions.

We refer to the model configuration for each of these problems as modes 1 through 5, respectively. Note that modes 2 and 3 compute wave structure and its corresponding growth rate which asymptotically becomes the fastest among the modes of the linear system (see Miller and Fehribach [11] for further details on the procedure). Mode 4 allows an arbitrary sequence of wavenumbers in the model. Mode 5 deals with a simple spectral truncation series with wavenumber being multiplied by a fixed harmonic factor. Therefore, in addition to the traditional spectral resolution 1 to K, the model can solve for the same number of wave components but in a higher harmonic; for example, the wavenumber set $\{5, 10, ..., 5K\}$ can be used, which imposes a five-fold symmetry upon the solution. In the mode 5 application, the well-known transform method (reviewed by McChenhauer [12]) is employed to compute the spectral transformations of nonlinear terms in the equations. Details of this method are given in Section 2.2.5.

The advantages of the hybrid technique should now be apparent. By using Fourier decomposition, the same model can be used to handle any of the above classes of problems. By using finite differences in the meridional plane and using spherical coordinates, one can consider a broad range of domains including a full sphere, a hemisphere (or any other sub-domain), a full cylinder, or a cylindrical annulus, and one can choose from a variety of boundary conditions.

2.2.1. *Spatial Discretization.* The meridional plane is partitioned into an arrangement of elements by defining grid intervals in the latitudinal and vertical directions. A staggered grid system similar to that of Quon [9] is employed. The variables u, T, and Π are defined in the center of the elements; v is defined at the middle of the vertical boundary of each element (i.e., on the sides), and w is defined at the middle of the top and bottom of each element. Note that the grid system includes artificial points outside the physical domain, for efficiency in computation and second-order accuracy in imposing the boundary conditions. The grid can be stretched in both directions, so that finer resolution can be obtained in regions of strong gradients (usually near the boundaries). The initialization routine of the model constructs a stretched grid which has grid spacings that are determined based on the formula $\sin(\pi\gamma) + \delta$. The variable γ is the dimensionless measure of physical distance between boundaries (ranging from 0 to 1), and δ is an input parameter. For larger δ, the grid stretching is less severe. There is also an input parameter which adjusts the location where the grid is to be stretched. This is done by shifting the phase of the sine function so that the desired amount of stretching in the location of interest is achieved. After the spacing function is determined, the grid intervals are multiplied by the appropriate constant such that they are in the proper units. The finite differencing is then performed upon the resulting grid. This method of achieving variable grid resolution differs from that of Quon, in which the equations are first transformed to a stretched coordinate system and then discretized with a constant interval. The advantage of the current method is its increased flexibility in the use of the same model code for a variety of geometries and flow types.

2.2.2. *Spatial Differencing.* The spatial derivatives in the discrete Fourier transformed equations are approximated by a control volume discretization procedure. Standard second-order centered difference approximations are used for the derivatives in each of the equations with the following exceptions.

For flows involving strong meridional circulations, numerical simulations using standard centered differences may result in artificial, small-scale features. Since most of the flows of interest to the authors involve a Prandtl number greater than one, this problem most often appears in the temperature field. Hence, the terms representing advection of heat by the mean meridional flow are evaluated as a weighted average of upwind and centered differences. The relative weights given to the two differences are an input parameter. A heavier weight on the upwind scheme may help suppress oscillatory behavior of the numerical solution. However, too much upwind differencing introduces artificial viscosity (see Roache [13]), which may degrade the accuracy of the solution. Thus, the requirement for upwind differencing must be evaluated for each individual problem. We have experimented with the use of centered differencing, upwind differencing, and an average of the two (with equal weight on each) for the case to be presented below. No *significant* difference was seen in the results as far as the conclusions stated or in the figures shown. However, when centered differencing was used for the multiple wave runs discussed later, non-physical, small-scale features are evident near the top of the domain, including the occurrence of temperature excursions beyond the range of the boundary values. We found that these anomalies can be eliminated by reducing the time step (from 0.10 to 0.05 s) *or* by using

upwind differencing. All results shown here use the former approach.

The second exception to the standard centered differencing formulation deals with the evaluation of the flux terms in the v and w equations. In that case, the Warn-Varnas *et al.* [14] "Scheme B" is used in order to conserve kinetic energy while retaining second order accuracy.

2.2.3. *Time Differencing.* A two-level scheme is used for the time differencing, which minimizes the computer memory requirements. First-order forward differencing is generally used, although exceptions to this rule are made according to numerical stability criteria. Those deviations are described in the following paragraphs.

In order to lessen the time step constraint due to the presence of inertial gravity waves, the Coriolis and the body force terms in the w and v equations use newly updated values of u and T (i.e., u and T are updated first before the tendencies of v and w are calculated). This introduces no complication for the axisymmetric part of the flow in which u is not involved in the continuity equation. However, mass continuity in the wave equations requires that all three velocity components be updated simultaneously, using an updated pressure field (see Section 2.2.4). In that case a tentative value of u, based upon the pressure at the previous time step, is used in the Coriolis terms for v and w. Experience has shown that the difference in the results obtained between this update procedure and the standard forward differencing scheme is insignificant, while the gain in allowable time can be sizable when the rotation rate or the vertical stratification is large.

To further permit longer time steps in some cases, there is an option of using ADI (alternating direction implicit) for the diffusion terms and those involving advection by the azimuthal mean flow. The ADI method treats terms implicitly in one direction and explicitly in the other direction at even time steps and reverses the directions of this treatment at odd time steps. The following is a description of the ADI method applied to the vertical direction at odd time steps, using the T equation as an example. Letting $n+1$ and n be the forecast and current time levels, respectively, the equation is discretized as follows:

$$\frac{\partial T}{\partial t} \approx \frac{\Delta T}{\Delta t} = \frac{T^{n+1} - T^n}{\Delta t} = -(D_r T^{n+1} + D_\phi T^n + D_\lambda T^n) + \kappa(L_r^2 T^{n+1} + L_\phi^2 T^n + L_\lambda^2 T^{n+1}) + \text{advection by other components.} \tag{2.6}$$

Here, D_λ, D_ϕ, and D_r represent the centered finite difference approximation of flux divergences due to the axisymmetric components of u, v, and w, respectively, and the L^2's represent the finite difference analog to the Laplacian components. The velocity components (evaluated at time level n) are included in our definitions of the D operators. The equations are rewritten in terms of ΔT and T^n. This is done by adding and subtracting the terms on the right hand side that are at time step n, then replacing $(T^{n+1} - T^n)$ with ΔT and gathering all the terms involving ΔT on the left hand side,

$$[1 - \Delta t(\kappa(L_r^2 + L_\lambda^2) - D_r]\,\Delta T = \text{discretized form of the complete right hand side of the temperature equation involving values at time step } n. \tag{2.7}$$

When (2.7) is expanded into matrix form, it is a tridiagonal matrix system for ΔT which is solved by the Gaussian elimination method. At even time steps, the r-derivatives on the left hand side are replaced by the ϕ-derivatives. Note that the λ part of the diffusion terms is implicit and the λ part of the advection terms is explicit at all time steps.

2.2.4. *Poisson Equation for Pressure.* At each time step, a pressure field must be found which results in mass continuity (zero divergence) for the new velocity field. The procedure is similar to that of Williams [6]. A Poisson equation is derived by first writing the momentum equations in vector form

$$\frac{\partial \mathbf{V}}{\partial t} = -\nabla \Pi + \mathbf{G}, \tag{2.8}$$

where $\mathbf{V}$ is the velocity vector and $\mathbf{G}$ represents the terms on the right hand sides of the momentum equations other than the pressure gradient terms.

Replacing the left hand side of (2.8) by forward differences and multiplying both sides by Δt gives

$$\mathbf{V}^{n+1} - \mathbf{V}^n = (-\nabla \Pi^* + \mathbf{G}^*)\,\Delta t, \tag{2.9}$$

where $n+1$ and n are the current and previous time steps, respectively. Π^* is the change in pressure from the previous time step, and the gradient of the old Π is included in the definition of $\mathbf{G}^*$. Applying the divergence operator to (2.9), setting the divergence of the new velocity vector to zero, and rearranging terms results in

$$\nabla^2 \Pi^* = \frac{\nabla \cdot (\mathbf{V}^n + \mathbf{G}^* \Delta t)}{\Delta t}. \tag{2.10}$$

Note that the term $\nabla \cdot \mathbf{V}^n$ is retained, since there is some round-off divergence from the previous time step.

The boundary condition used is that the normal derivative of Π^* is zero. This is consistent with our formulation of the pressure equation, in which the normal

derivative across the boundary is taken to be zero (justifiable because the momentum equation is not used to predict the boundary values). As explained by Williams [6], this condition results in Π^* being actually a quantity equal to the physical pressure correction except at the boundaries. A correction to Π^* could then be applied in order to recover the physical quantity; however, that step is not necessary, since the boundary derivative of Π is not required in solving the momentum equations.

The Poisson equation with the Neumann boundary condition is solved using a direct method that is vectorized for the CRAY-XMP (Sweet [15]). The solver has no problem with the fact that the solution for the axisymmetric component is not unique. It should be noted that the solution of the pressure equation is the most time consuming part of the model. For this reason, a control is provided that skips the pressure update if the maximum absolute value of the divergence is smaller than a prescribed (small) fraction of its ϕ component. This becomes particularly economical when long integrations are required for obtaining a steady state solution.

2.2.5. *FFT–Method for Computing Nonlinear Terms.* Around an azimuthal ring, every dependent variable is expanded in a discrete complex Fourier series as

$$q(\lambda_j) = \sum_{k=-K}^{K} Q_k \exp(ik\lambda_j), \tag{2.11}$$

where $\lambda_j = 2\pi j/L$ and K is the truncation limit of wavenumber k. The Fourier (or spectral) coefficients, $Q_k(r, \phi, t)$ are computed by the following:

$$Q_k = \frac{1}{L} \sum_{j=1}^{L} q(\lambda_j) \exp(ik\lambda_j). \tag{2.12}$$

Note that (2.12) is exact only if $q(\lambda_j)\exp(ik\lambda_j)$ is a truncated trigonometric series with maximum wavenumber less than or equal to $L-1$. Otherwise, aliases would result. Hence, if $q(\lambda_j)$ represents a product of two real variables representable by the same spectral series with truncation K, then $L \geqslant 3K+1$ must be satisfied. The actual calculations of (2.11) and (2.12) are carried out by a vectorized fast Fourier transform (FFT) algorithm (Temperton [16]). This FFT is the same as that used by the NCAR Community Climate Model which limits L to have multiplication factors of 2, 3, and 5 only. This does not place a constraint upon K, however, only a finite set of optimal values for L as a function K are tabulated in the program.

The Fourier transform method described above is efficient in dealing with the nonlinear (quadratic) terms in the governing equations (2.1)–(2.4). In short, all variables required in the calculations are first synthesized into physical space, where the quadratic factors (e.g., uv, v^2, vT, etc.) in the nonlinear terms are calculated. The spectral coefficients of those terms are calculated using the FFT. These spectral coefficients are then used in the finite differencing scheme to obtain the nonlinear tendencies for each wave component. Note that the FFT is used only when a fully nonlinear run of the model is made (mode 5). In mode 4, the nonlinear terms (which do not involve wave-wave interactions) are calculated in spectral space, on the r–ϕ grid.

2.2.6. *Polar Cases.* While the case considered here is an annulus which does not have a pole, we describe the procedure when there is a pole in the domain for the sake of completely describing the numerical model for future reference. The pole is a singular point in the coordinate system (i.e., the horizontal velocity components are not well defined there), although there are no physical constraints on the flow. Fortunately, the grid is structured such that a polar boundary condition is required only for the v-component of velocity. The values for the other variables are arbitrary because they are multiplied by zero in the finite difference scheme. However, the polar value of v is used in the calculation of viscous stress $\frac{1}{2}$ grid interval from the pole in order to calculate the viscous tendency for v at the point 1 grid interval from the pole. By considering a small neighborhood of the pole, it is easily shown that the only Fourier component which contributes to a non-zero flow at the pole is the wavenumber one component. Therefore, the condition used for the axisymmetric and all wave components except wavenumber one is $v = 0$ at the pole. For the wavenumber one component, the boundary condition used is zero meridional gradient. This arises from the facts that the flow resulting from the wavenumber one component is symmetric across the pole and must have a finite Cartesian derivative (in any direction) at the pole. The zero meridional derivative is approximated by setting the polar value equal to the value 1 grid point from the pole, which is only first-order accurate. Physically, this equates to assuming no viscous stress on the cross-polar component of the flow.

2.3. *Model Validation*

The validation of the model includes the results presented in Section 3 and other numerical simulations of laboratory experiments in either cylindrical or spherical geometry. Miller and Butler [17] used the present model in modes 1–4 to calculate the transition between axisymmetric and wave flow as seen in the annulus experiments of Fein [18], including hysteresis of the upper transition in the free-slip upper surface case. Excellent agreement was obtained, with the exception of rapidly rotating cases in which curvature effects on the free surface neglected by the model could be important. Comparisons with numerical simulations by

Hignett *et al.* [21] resulted in excellent agreement for two steady-wave cases in a rigid-lid annulus. We have also conducted numerical studies on the amplitude vacillation phenomena (Pfeffer *et al.* [22]) and found very good agreement with the laboratory experiments. In numerical simulations of the rotating hemispherical experiments of Hart *et al.* [19], we obtained time-dependent solutions which agreed with calculations using the model of Glatzmaier [20] with identical initial conditions. The spherical results and those on vacillation in the cylindrical annulus will be discussed in other papers.

3. THE WILLIAMS STEADY WAVE CASE

3.1. *Comparisons of Equilibrated Flow*

Extensive model validations were performed for the steady-wave case of Williams [6–8] and Quon [9]. In all the results presented here, the number of grid points is 26 in both the radial and vertical directions (24 intervals between the physical boundaries). The grid is stretched such that the smallest grid interval near the boundaries is about half of the largest interval in the center of the annulus. Our chosen grid resolution is comparable to those used by Williams and Quon, although Quon selected a higher stretching factor near the boundary, and Williams had more grid points (33), with constant intervals. Note that Quon's model is essentially the same as the present model in mode 4 with a single wave 5, while the Williams model is similar to the present model in the fully nonlinear mode. The model was also run in mode 1 to generate a steady axisymmetric solution and in mode 2 to compute the stability analysis with respect to the basic state given in the axisymmetric solution. In all cases, the model was integrated for a long enough time that the flow was virtually equilibrated (generally ~ 130 rotations).

As shown in Fig. 1, the axisymmetric solution consists of a strong westerly jet at the top of the annulus, prevailing easterlies over the lower surface, and an absence of the Ferrell cell. These results agree with similar calculations by both Williams and Quon. Figure 1 also shows the temperature wave amplitude function for wave 5, which is one of the unstable eigenmodes associated with the given linear system. The corresponding growth rate ($0.035\ s^{-1}$) is actually smaller than that of wave 4, which is $0.044\ s^{-1}$.

In order to simulate the five-fold symmetry assumed by Williams, the model was run in fully nonlinear mode with waves 5, 10, and 15 present. Several initial conditions were used which resulted in the same equilibrated flow, including (1) the steady axisymmetric solution and a small amplitude and point perturbations in the temperature fields of each wave, and (3) the state of no motion and isothermal interior, with point perturbations in temperature for each of the waves. The equilibrated solution, which is shown in Fig. 2, is virtually identical to that of Williams and similar to that of Quon. It is seen that westerlies extend to the surface and a strong Ferrell cell forms in the middle of the annulus. The zonal jet is reduced by 40%, from $0.52\ cm\ s^{-1}$ in the axisymmetric solution to $0.30\ cm\ s^{-1}$. The maximum wave temperature amplitude is about 0.72°C, and the relative size of the local maximum in the temperature wave amplitude near the inner wall is reduced considerably from that of the linear eigenmode (compare Figs. 1D and 2D). The effects of spectral truncation on the solutions were also examined by varying the number of waves, still assuming five-fold symmetry. Only minor differences were detected among the cases in which one or more harmonic waves were included with the fundamental wave 5 (see Table II).

In an attempt to reproduce the results in Quon [9], the model was also run in mode 4 with wave 5 only present. As in the fully nonlinear cases above, a variety of initial conditions were used, and no effect upon the equilibrated flow was observed. The resulting equilibrated azimuthal mean state and temperature wave amplitude are shown in Fig. 3. The maximum temperature amplitude near the center of the annulus is 0.5°C, which is about 40% smaller than that estimated from Fig. 8 in Quon's paper. Smaller wave amplitude gives rise to weaker wave-mean interactions than in the fully nonlinear case. In comparison with the axisymmetric solutions shown in Fig. 1, the zonal jet is reduced by only about 10%, in comparison with 40% in the fully nonlinear runs. The formation of the Ferrell cell is far less vigorous and is confined in the upper part of the fluid domain. The surface flow in the middle of the annulus remains easterly in contrast to westerly seen in Fig. 2 and in Quon's results. Other runs with wave 5 only indicate that these results are insensitive to grid resolution.

We also ran the present model with the single wave 4 rather than wave 5. The resultant azimuthal mean state and wave amplitude were found to be more similar to the results of Williams and Quon than is the single wave 5 case shown above. A relevant point to note is that the amplitude of single wave 5 vacillates for a relatively long time before

TABLE II

Selected Results of Calculations

Wave(s)	U_{max}	U_{min}	ψ_{max}	ψ_{min}	$\lvert V\rvert_{max}$	$\lvert T_k\rvert_{max}$	Nu
None	0.52	−0.077	0.031	0.0	0.52	—	3.30
5	0.47	−0.082	0.038	−0.001	0.60	0.49	4.59
5, 10	0.34	−0.092	0.046	−0.014	0.55	0.71	6.32
5, 10, 15	0.30	−0.100	0.048	−0.017	0.51	0.72	6.73
4	0.39	−0.084	0.044	−0.012	0.63	0.85	5.91
4, 8	0.27	−0.105	0.052	−0.021	0.54	0.95	7.17
4, 8, 12	0.27	−0.106	0.053	−0.023	0.54	0.93	7.23

Units. U, $|\mathbf{V}|$, $cm\ s^{-1}$; ψ, $cm^3\ s^{-1}$; T, °C; Nu, dimensionless.

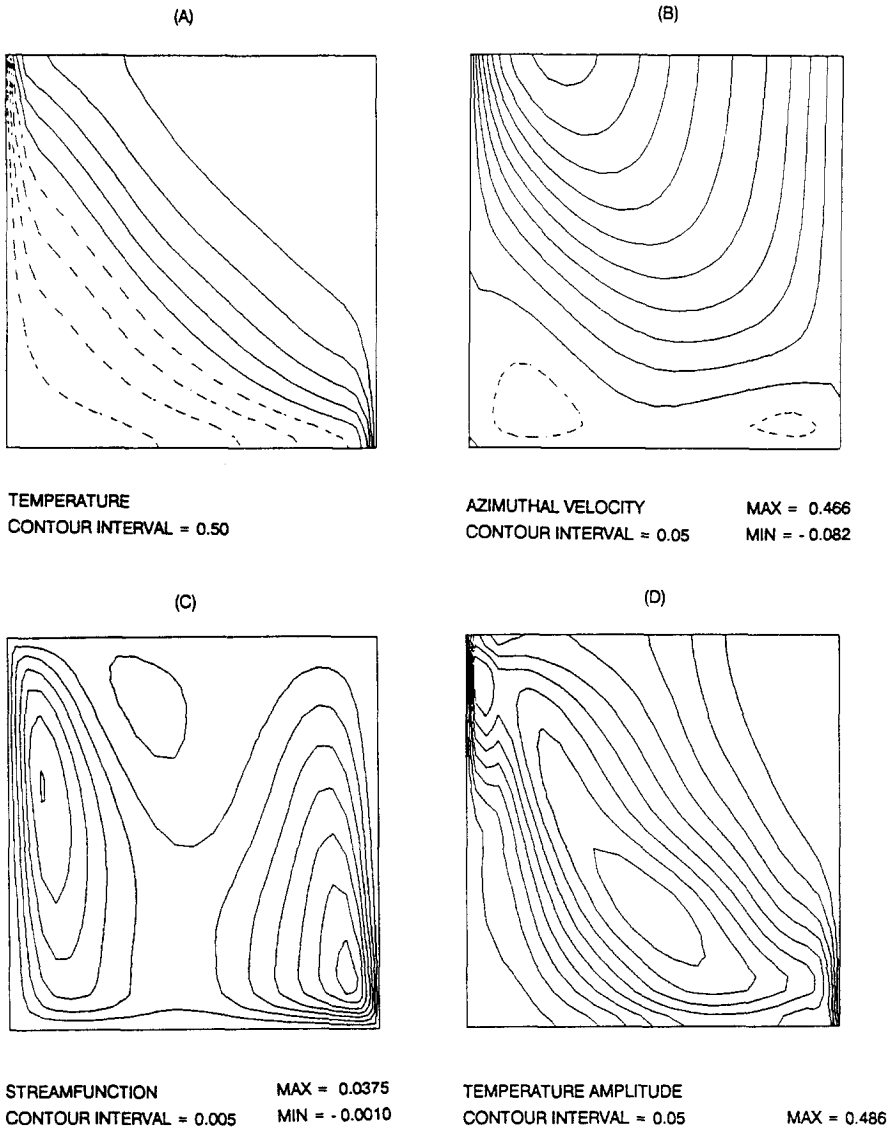

FIG. 3. Calculated azimuthal mean fields for the calculation which used only wave 5 to represent the azimuthal variations. Panels (A) through (D) are as in Fig. 2.

equilibrating to a steady state, while the single wave 4 equilibrates rapidly with fewer vacillation cycles (see Fig. 4). The integrations that resulted in Fig. 4 were initialized with the steady axisymmetric state plus the corresponding linear eigenmodes with small amplitude, the latter having been obtained from mode 2 integrations.

Table II summarizes the results discussed above in terms of maximum and minimum azimuthal velocity (U) and meridional streamfunction (ψ) of the azimuthal mean flow, maximum flow speed ($|\mathbf{V}|$), maximum temperature amplitude of the dominant wave ($|T_k|$), and Nusselt number (Nu—ratio of the integrated boundary heat flux to that of a conductive equilibrium state). The streamfunction is the negative of that defined by Williams [7] and Quon [9].

3.2. *Wavenumber Selection*

Several additional experiments were conducted to investigate the behavior of wavenumber selection. In two experiments, the initial condition for all waves was very small point perturbations in the temperature field, and the steady axisymmetric solution was used for the initial axisymmetric part of the flow. The first experiment was conducted with the model in mode 4 with waves 4 and 5 only, and the other in mode 5 with waves 1 through 15. In both cases, wave 4 eventually dominated and the contribution from wave 5 was negligible. The equilibrated flow with 15 waves present was essentially identical to that when waves 4, 8, and 12 only were used. The selection of wave 4 at this point in parameter space contrasts with the selection of

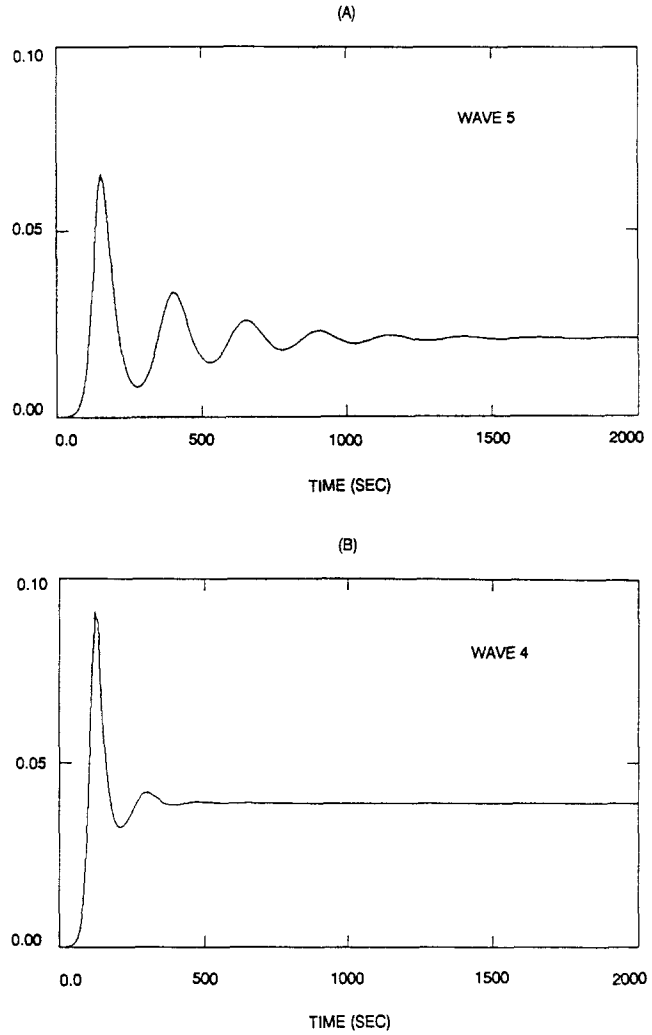

FIG. 4. Wave kinetic energy as a function of time for two single-wave calculations: (A) wave 5; (B) wave 4.

wave 5 indicated by Williams [7], who conducted preliminary calculations in the full annulus domain using "medium resolution." The different result does not necessarily represent a disagreement between the two models, since the issues of initial conditions and grid resolution (which were not specified by Williams) may play important roles in the wavenumber selection.

In another set of two experiments with the model in fully nonlinear mode (15 waves), we found that wave 5 retains dominance when it is dominant in the initial conditions. The initial conditions used in these calculations were equilibrated wave-5 flows: (1) the single-wave-5 solution and (2) the multiple-wave solution (waves 5, 10, and 15). Waves 1–4 were initially given small point perturbations in the temperature field. The resulting equilibrated flows in these two experiments were essentially the same as that for the run with waves 5, 10, and 15 only present. The fact that the dominant wave in the equilibrated flow depends upon the initial conditions is analogous to hysteresis phenomena that have been frequently observed in laboratory experiments (e.g., Fein [18], Hignett *et al.* [21]). This result suggests that hysteresis is a possible reason for the discrepancy in wavenumber selection between our calculations described in the preceding paragraph (i.e., when the initial amplitudes of all waves are small) and Williams' [7] result. Williams did not give information on the initialization procedure for his preliminary calculations in the full annulus domain. If he had initialized the calculation with a previous result in which wave 5 was dominant (perhaps from a nearby point in parameter space), then wave 5 may have continued to dominate because of the hysteresis effect.

Other calculations indicate that the hysteresis in wavenumber selection for this case occurs only when using a fully nonlinear model. In initial value experiments with waves 4 and 5 only (no wave–wave interaction), we found that wave 4 eventually becomes dominant and wave 5 decays regardless of the relative sizes of initial amplitudes given to these two waves. This is not to imply, however, that hysteresis in general is a result of wave–wave interactions. As pointed out earlier, Miller and Bulter [17] simulated a hysteresis phenomenon observed in the laboratory experiments of Fein [18] by using the present model in mode 4, i.e., in which only wave–mean interactions were involved.

4. SUMMARY

We have described a newly developed numerical model for studying buoyantly driven, rotating flows in spherical and cylindrical geometries when the Boussinesq approximation is valid and when centrifugal effects upon the free upper surface can be ignored. The model uses a hybrid spectral and finite difference technique to approximate the governing differential equations. Because of the flexibilities in the choices of geometric framework and boundary conditions, the present model is suitable to simulate the flows observed in the rotating annulus experiments (either side-heated or bottom-heated), and in the Spacelab Geophysical Fluid Flow Cell experiment (Hart *et al.* [19]). The model also allows various modes of integrations which are useful for conducting sensitivity experiments and performing linear stability analyses.

Calculations have been performed to reexamine the steady baroclinic wave case of Williams [6–8] and Quon [9]. Excellent agreement between the present model and that of Williams is achieved when 1 or more harmonic waves are included with the fundamental wave 5 in the fully nonlinear model integrations. However, a significant disagreement between the present model and Quon [9] is obtained when only wave 5 is considered. The disagreements are seen in the smaller wave amplitude and consequently in a much smaller effect upon the azimuthal mean state than those obtained by Quon. Since the equations and numerical technique used by Quon are essentially the same

as the present model, the reasons for the discrepancy are not evident. Because the present model agrees very well with the Williams results and with the laboratory experiments of Fein [18] (see Miller and Butler [17]), the discrepancies appear to cast some doubt upon the validity of Quon's solution.

In the 15-wave, fully nonlinear integrations, the equilibrated solution of the Williams case depend upon initial conditions. Wave 4 eventually dominates if all wave amplitudes are initially very small. Wave 5 continues to dominate if the initial amplitude of wave 5 is large and that of wave 4 is small. The Williams steady wave case is identified as a case of multiple equilibria in which there exists hysteresis in the wavenumber selections. Similar calculations in which wave–wave interactions were omitted did not result in hysteresis.

Many numerical studies for the rotating annulus experiments and for the spherical Spacelab experiments using the present model are underway. The model's capability makes it a valuable tool to examine some very interesting geophysical flow problems such as hysteresis, amplitude vacillation, structural vacillation, and geostrophic turbulence (Pfeffer *et al.* [22]). The results of these studies can be applied toward improving our understanding of the dynamics of earth's atmosphere and oceans.

ACKNOWLEDGMENTS

Modeling and Data Assimilation Programs, at NASA Headquarters.

REFERENCES

1. J. G. Charney, *J. Meteorol.* **4**, 135 (1947).
2. E. T. Eady, *Tellus* **1**, 33 (1949).
3. E. N. Lorenz, *The Nature and Theory of the General Circulation of the Atmosphere* (World Meteorological Organization, Geneva, 1967), p. 78.
4. R. L. Gall, *J. Atmos. Sci.* **33**, 374 (1976).
5. W. W. Fowlis and R. Hide, *J. Atmos. Sci.* **22**, 541 (1965).
6. G. P. Williams, *J. Fluid Mech.* **37**, 727 (1969).
7. G. P. Williams, *J. Fluid Mech.* **49**, 417 (1971).
8. G. P. Williams, *Mon. Weather Rev.* **100**, 29 (1972).
9. C. Quon, *J. Comput. Phys.* **20**, 442 (1976).
10. T. L. Miller and R. L. Gall, *J. Atmos. Sci.* **40**, 2293 (1983).
11. T. L. Miller and J. D. Fehribach, *Geophys. Astrophys. Fluid Dyn.* **52**, 25 (1990).
12. B. McChenhauer, in *Numerical Methods Used in Atmospheric Models, Vol. II* (GARP Publication Series No. 17, World Meteorological Organization, Geneva, 1979), p. 124.
13. P. J. Roache, *J. Comput. Phys.* **10**, 351 (1972).
14. A. Warn-Varnas, W. W. Fowlis, S. Piacsek, and S. M. Lee, *J. Fluid Mech.* **85**, 609 (1978).
15. R. A. Sweet, *SIAM J. Sci. Stat. Comput.*, **9**, 761 (1988).
16. C. Temperton, *J. Comput. Phys.* **52**, 198 (1983).
17. T. L. Miller and K. A. Butler, *J. Atmos. Sci.* **48**, 811 (1991).
18. J. S. Fein, *Geophys. Fluid Dyn.* **5**, 213 (1973).
19. J. E. Hart, G. A. Glatzmaier, and J. Toomre, *J. Fluid Mech.* **173**, 519 (1986).
20. G. A. Glatzmaier, *J. Comput. Phys.* **55**, 461 (1984).
22. R. L. Pfeffer, G. Buzyna, and R. Kung, *J. Atmos. Sci.* **37**, 2129 (1980).